

BRIEF COMMUNICATION OPEN ACCESS

# Induced and Transferred Charge in Dielectric-Barrier Discharge Setups Without 2D-Translational or Cylindrical Symmetry

Claus-Peter Klages  | Lars Bröcker 

Institute for Surface Technology, IOT, Technische Universität Braunschweig, Braunschweig, Germany

**Correspondence:** Claus-Peter Klages ([c-p.klages@tu-braunschweig.de](mailto:c-p.klages@tu-braunschweig.de))**Received:** 9 December 2024 | **Revised:** 19 February 2025 | **Accepted:** 14 March 2025**Funding:** The work is funded by the Deutsche Forschungsgemeinschaft (DFG, German Research Foundation) (Project Number: 504701852).**Keywords:**  $\lambda$  function | dielectric-barrier discharge | equivalent electric circuit | Green's reciprocity theorem | induced charge | transferred charge

## ABSTRACT

For dielectric-barrier discharges (DBDs) in setups lacking 2D-translational or cylindrical symmetry, an electrical analysis within the framework of a 3-capacitor equivalent-circuit model is no longer possible. In this situation, it makes sense to adapt an approach developed in the late 1980s for analyzing partial discharges in high-voltage systems, based on the so-called  $\lambda$  function, or alternatively to apply a fundamental theorem of electrostatics directly, on which this function is also based. The main purpose of this short communication is to draw the attention of the scientific community of researchers interested in DBDs to the existence of a very useful concept, published decades ago in the electrical engineering literature and apparently still little known in this community.

## 1 | Motivation

The considerations reported in this communication were motivated by studies on plasma deposition of thin films from Ar-based mixtures with fractions  $x_p$  of various precursors in pin-to-plate dielectric-barrier discharges (DBDs), with pin electrodes covered by a planar dielectric (Figure 1I) [1, 2]. With a rapid transverse gas flow (typical average velocity  $v_{av} = 50$  cm/s) through the gas gap (typical width  $g = 2.5$  mm), film deposition is predominantly due to cations that arrive at the temporary cathode during transient micro-discharges [1–3]. For most of the applied organosilane or siloxane precursors, the positive-ion production in gas mixtures with  $x_p$  between about 10 ppm and a few 1000 ppm is dominated by Penning ionization, and precursor-derived cations are prevalent in the total cation flux to the temporary cathode.

To determine the ion charge  $q$  transferred simultaneously with a certain increment of film mass on the temporary cathode during a transient microdischarge from current or charge

measurements, a suitable model must be applied. A typical Lissajous or  $Q(U)$  figure obtained by plotting the charge  $Q$  on a measuring capacitor as a function of the applied voltage  $U$  is shown in Figure 1II.

Now the question arises how the externally measurable charge  $Q$  is related to the charge  $q$  transferred in the discharge to the electrode surfaces. Unfortunately, the equivalent-circuit approach, commonly applied to answer this question, fails for the used setup as it will be explained below, based on Figure 2.

The sketches in this figure show various setups in which steady DBDs can be sustained. For many more configurations used so far, see Brandenburg [4]. Arrangements I and II are of practical interest to generate large-volume DBDs between large-area planar electrodes (I) or in long cylindrical setups (II). Discharges in dielectric-surrounded voids (III), on the other hand, are examples of a large variety of “partial discharges” (PDs), known in electrical engineering since about one century (see Hauschild and Lemke [5, pp. 157–160] and Niemeyer [6]). IEC<sup>1</sup>

This is an open access article under the terms of the [Creative Commons Attribution](https://creativecommons.org/licenses/by/4.0/) License, which permits use, distribution and reproduction in any medium, provided the original work is properly cited.

© 2025 The Author(s). *Plasma Processes and Polymers* published by Wiley-VCH GmbH.

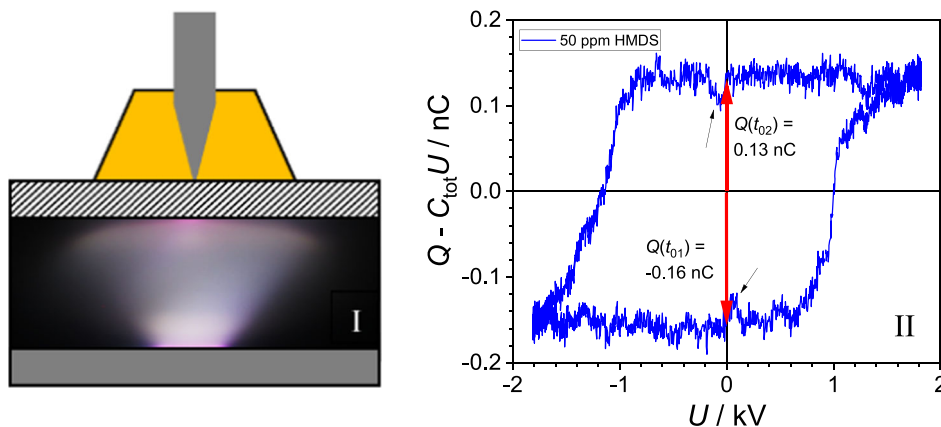


**FIGURE 1** | (I) Photograph of a typical discharge in the pin-to-plate DBD used in Bröcker et al. [1], with glass dielectric (dashed), Si ground electrode (gray), and a sharpened pin as high-voltage electrode (gray, length  $L = 30$  mm,  $x_p = 50$  ppm HMDS/Ar, amplitude of applied sinusoidal voltage  $U_0 = 1.75$  kV, frequency  $f = 19$  kHz, mean gas flow velocity  $v_{av} = 50$  cm/s). (II) Lissajous figure: from the charge  $Q$  on the measuring capacitor ( $C_m = 1$  nF), the product  $C_{tot}U$  ( $C_{tot}$  depends on  $L$ ; with  $L = 50$  mm,  $C_{tot} = 1.5$  pF) was subtracted to improve the visibility of the relatively small discharge-induced charge increments  $\Delta Q$  near  $|U| = 1$  kV ( $|\Delta Q| = 0.29$  nC, vs.  $C_{tot} \cdot 1$  kV = 15 nC). (The cause of the small dips in  $Q - C_{tot}U$  near  $U = 0$  V (black arrows) is so far unknown.)

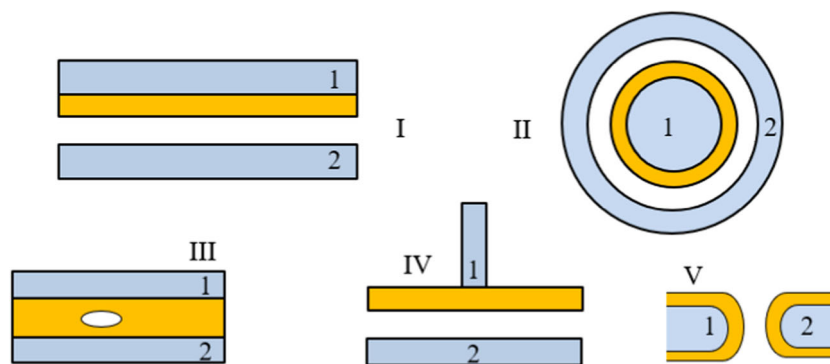


**FIGURE 2** | Arrangements of two electrodes with intermediary dielectric layers (orange) and gas gaps or gas-filled void (cross sections). (I) 2D-extended planar arrangement. (II) Long cylinder. (III) Void in a dielectric, filling the space between two electrodes. (IV) Pin-to-plate arrangement, dielectric-covered pin. (V) Pin-to-pin arrangement, dielectric-coated pins.

standard 60270:2000 defines PDs as “localized electrical discharges that only partially bridge the insulation between conductors”<sup>2</sup> [5, p. 158]. Arrangements like IV or V are used to study DBDs with small gas residence times [1, 2] or DBDs consisting of single discharge filaments [7].

There is an important difference between designs I and II on the one hand and III, IV, V on the other: due to the virtual 2D-translational symmetry of I and the cylindrical symmetry of II<sup>3</sup>, all points of the dielectrics’ surfaces are equivalent and, with a voltage  $U$  between electrodes 1 and 2, on the same electric potential  $\phi$ . Therefore, a virtual third conductor can be applied along these surfaces without changing capacitances  $C_I$  or  $C_{II}$ . With three conductors, two capacitances can be defined: That is why  $C = C_I$  or  $C_{II}$  can be calculated by Equation (1), representing a serial connection of a capacitor completely filled by the dielectric with capacitance  $C_d$ , and an “empty” capacitor with capacitance  $C_g$ :

$$C = \frac{C_d C_g}{C_d + C_g}. \quad (1)$$

Due to the lack of the required symmetry, that is not possible for setups III, IV, and V.

## 2 | Equivalent Electric Circuits for DBDs

The difference between the two types of partially filled capacitors described in the previous chapter is of considerable importance for electrical discharge modeling of discharges by equivalent electric circuits, applied for the first time in 1928 to study gas breakdown in voids in laminated insulators, see Hauschild and Lemke [5, pp. 161–164].

The simplest equivalent circuit model for a DBD cell comprises two capacitors  $C_g$  and  $C_d$  in series, and parallel to  $C_g$ , as an element representing the discharge, a “black box” [8], a variable resistor [4, 9], or a current source [10], as in Figure 3 (without the capacitance  $C_s$ ).

To describe real DBD devices, various reasons require a modification of this equivalent circuit: Stray (or parasitic) capacitances

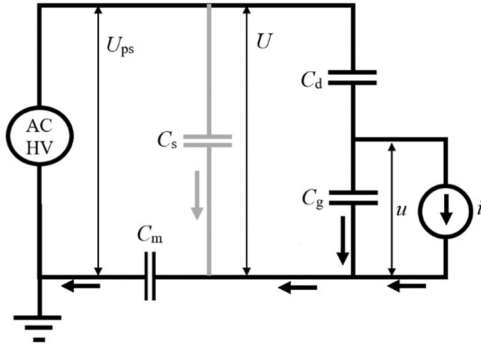


**FIGURE 3** | Equivalent electric circuit for a DBD in setup I or II.  $i$  and  $u$  are discharge current and gap voltage, respectively. Voltages  $U$  and  $U_{ps}$  (terminal voltage of the high-voltage power source “AC HV”) are virtual equal, when the measuring capacitor  $C_m$  is chosen large enough. See the text for further explanation.

$C_s$  due to unavoidable proximity of conductors on different potentials can be caused by cables, high-voltage connections, or throughputs. Not-discharged parts of a gas gap are electrically equivalent to stray capacitances and can likewise be accounted for by one or several parallel capacitances [8, 11, 12].

In high-voltage engineering, equivalent circuits with three capacitances, also known as “abc models” due to their common names  $C_a$ ,  $C_b$ ,  $C_c$ , have been used to model PDs since the 1950s (see Hauschild and Lemke [5, pp. 160–170] and Whitehead [13]). Main objective of such models has been to relate externally measurable “apparent” charges to “true charges” transferred by PDs, for example, in micro-cavities in an insulating material.

Relations between internal, discharge-related quantities like discharge current  $i(t)$ , gap charge  $q(t)$ , gap voltage  $u(t)$ , and measured or given quantities  $Q(t)$ ,  $I(t)$ , and  $U(t)$  can be obtained by extending the equivalent circuit of Liu and Neiger [10] by a capacitance  $C_s$ . The resulting Equations (1)–(2) agree with equations given before in other papers in different notations ( $C_{cell} \equiv C_g C_d / (C_g + C_d)$ ;  $C_{tot} \equiv C_{cell} + C_s$ ) [8, 11].

$$i(t) = \left( \frac{1}{1 - C_{cell}/C_d} \right) \cdot \left( I(t) - C_{tot} \frac{dU(t)}{dt} \right); \quad (2)$$

$$q(t) = \left( \frac{1}{1 - C_{cell}/C_d} \right) \cdot (Q(t) - C_{tot} U(t)); \quad (3)$$

$$u(t) = \frac{1}{C_d} \cdot [(C_d + C_s)U(t) - Q(t)]. \quad (4)$$

During one period of duration  $T$  of an applied ac voltage (e.g., a sinusoidal voltage), there are two points in time ( $t_{01}$  and  $t_{02} = t_{01} + T/2$ ) when  $U = 0$  and the ratio  $Q(t_{01})/q(t_{01}) = Q(t_{02})/q(t_{02})$  is a constant depending only on capacitances  $C_{cell}$  (or  $C_g$ ) and  $C_d$  (Equation 3). For the differences  $\Delta Q_0 \equiv Q(t_{01}) - Q(t_{02})$  (Figure 111) and  $\Delta q_0 \equiv q(t_{01}) - q(t_{02})$  follows

$$\Delta Q_0 = (1 - C_{cell}/C_d) \cdot \Delta q_0 = \left( \frac{1}{1 + C_g/C_d} \right) \cdot \Delta q_0 = \left( \frac{C_{cell}}{C_g} \right) \cdot \Delta q_0. \quad (5)$$

In the electrical-engineering literature, a Danish group of authors criticized the capacitance-based equivalent-circuit approach since the late 1980s, arguing that it does not correctly reflect the physics of PDs [14, 15]. In fact it must be noted that Equations (2)–(5) are based on the separability of  $C_{cell}$  into  $C_d$  and  $C_g$  which is not given for arrangements III–V of Figure 2.

### 3 | Induced Charge $Q$ via Pedersen's $\lambda$ Function

Pedersen and colleagues published an alternative to the “abc model” of PDs, based on fundamental field-theoretical arguments [14–16]. Relevant articles appeared only in the electrical-engineering literature and are apparently still hardly known in the community of researchers and engineers interested in DBDs.

In the alternative approach, a dimensionless scalar-field function  $\lambda$  plays a central role.

$\lambda_i$  is defined as the electric potential distribution in a system

- with at least two electrodes  $E_1$  and  $E_2$  and one or more dielectrics  $D$ ,
- without any free charges (as opposed to polarization charges) such as surface charges on dielectrics or volume charges in the gas phase,
- with a potential of  $\phi_i = 1V$  on electrode  $i$  while other electrodes are grounded,

divided by  $\phi_i$ .

Then, in the absence of any space charges between the electrodes<sup>4</sup>, a surface charge density distribution  $\sigma$  on the dielectric(s) will induce a charge  $Q_i$  on the electrode  $i$ , whereby

$$Q_i = - \int_D \lambda_i \sigma \, ds. \quad (6)$$

The integral extends over the whole surface  $D$  [14].

An application of this equation to a pin-to-plate arrangement with a dielectric-covered pin (Figure 11V) as the single dielectric will be outlined further below. Equation (6) can, however, also be applied to setups with dielectrics covering both electrodes.

### 4 | Induced Charge $Q$ From Green's Reciprocity Theorem

Equation (6) can alternatively be obtained by applying Green's reciprocity theorem<sup>5</sup> (1828), on which Pedersen's approach is also based, directly to the system of electrodes and dielectric(s) considered above. Clemmow gives a very concise formulation of the theorem [18]: If charge densities  $\rho$  and  $\rho'$  separately give rise to respective potentials  $\phi$  and  $\phi'$ , then

$$\int_V \rho \phi' \, dv = \int_V \rho' \phi \, dv, \quad (7)$$

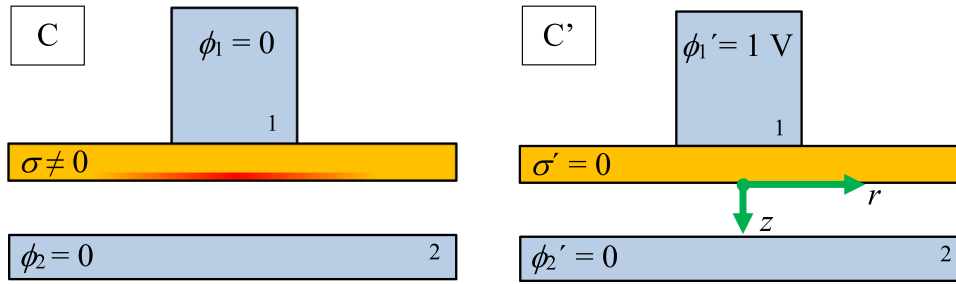


**FIGURE 4** | Two different configurations C, C' of potentials  $\phi$  on electrodes  $E_1, E_2$  (blue) and charge densities  $\sigma$  on the surface of a dielectric D (orange). C represents the experimental situation of a pin-to-plate DBD with a pin-backed dielectric after a discharge has left behind charges (red) on D, while the applied voltage is crossing zero. C' is the configuration for which the electric potential  $\phi'$  on the surface of D is calculated to obtain the  $\lambda_1$  function by division through 1 V.  $r, z$  (green) refer to cylinder coordinates used in Section 5.

where the volume integrals are over all space V. The validity of Equation (7) for systems with dielectrics was shown by Smythe [19]; Clemmow gives the proof in a different notation [18].

Figure 4 shows configurations C and C' for a pin-to-plate arrangement with two electrodes  $E_1$  and  $E_2$  and an interposed dielectric D. Spatial distributions of charge densities  $\rho$  and  $\rho'$  and potentials  $\phi$  and  $\phi'$  are chosen as follows:

- C: Nonzero surface charge distribution  $\sigma$  on the dielectric's D surface, value of potential distribution  $\phi$  at both electrodes  $E_1, E_2$ :  $\phi = 0$
- C':  $\sigma' = 0$  on D, value of potential distribution  $\phi'$  on electrodes:  $\phi'_1 = 1$  V and  $\phi'_2 = 0$

Again, the gas phase is considered to be free of charge. As charges can reside either on the electrodes E or on the dielectric D, both integrals in Equation (7) can be split into two parts, one for E (including contributions from  $E_1$  and  $E_2$ ) and one for D. Charges  $\sigma$  on D are assumed to reside only on its surface, the volume of D is assumed to be charge-free.

Then the volume integrals over the dielectric D are reduced to surface integrals over its surface ( $d\tau =$  differential area):

$$\int_E \rho \phi' dv + \int_D \sigma \phi' d\tau = \int_E \rho' \phi dv + \int_D \sigma' \phi d\tau, \quad (8)$$

E : electrodes, D : dielectric.

The 3rd and the 4th integral in Equation (8) are zero because  $\phi = 0$  on both electrodes and  $\sigma' = 0$  on D. Only  $E_1$  contributes to the first integral, because  $\phi'_2 = 0$ .  $E_1$  is on a spatially constant potential  $\phi'_1 = 1$  V which can be placed in front of the integral, the remaining volume integral represents the charge  $Q_1$  induced on  $E_1$  by the charge density  $\sigma$  on D:

$$\phi'_1 \int_E \rho dv = (1V) \cdot Q_1 = - \int_D \phi' \sigma d\tau. \quad (9)$$

In contrast to the potentials of conductors  $E_1$  and  $E_2$ ,  $\phi'$  on the surface of the insulator D in the pin-to-plate arrangement is location-dependent, due to the lack of 2D-translational or

cylindrical symmetry. Dividing this potential through 1 V results in  $\lambda_1$  as defined in Section 3:

$$Q_1 = - \int_D (\phi'/1V) \sigma d\tau = - \int_D \lambda_1 \sigma d\tau. \quad (10)$$

Equation (10) equals Equation (6) for the case of  $i = 1$ .

## 5 | Application to Arrangements I or II, and IV—Transferred Charge

Arrangements I and II are basically plate- or cylindrical capacitors that are partially filled with dielectrics. Since here the surfaces D of the dielectrics are on a location-independent potential,  $\lambda_1$  is constant and can be placed in front of the integral in Equation (10). The remaining integral equals  $q$ , the total surface charge on D. Equation (1) can now be applied to calculate the capacity  $C_{\text{cell}}$  of the capacitor, and it follows from the voltage division in that capacitor that  $\lambda_1$ , that is, the voltage at the gap/dielectric interface for potentials of 1 V at electrode 1 and 0 V at electrode 2, divided by 1 V, equals  $C_{\text{cell}}/C_g$ :

$$Q_1 = - \lambda_1 \cdot \int_D \sigma \cdot ds = - (C_{\text{cell}}/C_g) \cdot q. \quad (11)$$

Equation (11) is—apart from the sign, which actually must be negative—in agreement with Equation (3) at  $U = 0$ . Note that this equation holds for any spatial distribution of the charge  $q$  on D—also, for example, for a localized charge left behind from a single microdischarge.

As for other arrangements, a relatively simple expression can be obtained for  $Q_1$  in case of axial symmetry like pin-to-plate arrangements with an interposed dielectric contacting electrode 1 like in Figure 4 where the origin and coordinates  $r$  and  $z$  of a system of cylindrical coordinates  $r, \theta, z$  are indicated for configuration C'. If the radius of the dielectric disc  $r_D$  is large compared with the radial extension of the discharge so that no charge is deposited on the disk's edge or its upward facing surface, it suffices to integrate over  $\theta$  and  $r$  at  $z = 0$  in the system of cylinder coordinates  $r, \theta, z$  (see Figure 4C'), to calculate  $Q_1$  from Equation (10). This will capture all charges left behind on the part of the dielectric's surface D which is downward orientated in Figure 4, facing the grounded electrode 2:

$$\begin{aligned}
 Q_1 &= - \int_0^{2\pi} \int_0^{r_D} \lambda_1(r, \theta, 0) \sigma(r, \theta, 0) r \, d r \, d \theta \\
 &= -2\pi \int_0^{r_D} \lambda_1(r) \sigma(r) r \, d r
 \end{aligned} \tag{12}$$

or, with the normalized surface charge density distribution  $\sigma_n(r)$ , defined as

$$\sigma_n(r) = \sigma(r) / \left( 2\pi \int_0^{r_D} \sigma(r) r \, d r \right) = \sigma(r) / q \tag{13}$$

$$Q_1 = - \left( 2\pi \int_0^{r_D} \lambda_1(r) \sigma_n(r) r \, d r \right) \cdot q \equiv -B_1 \cdot q. \tag{14}$$

The bracketed term in Equation (14), here provisionally abbreviated  $B_1$ , plays the role of the expression  $(1 - C_{\text{cell}}/C_d) = C_{\text{cell}}/C_g$  in Equation (3). Note that  $B_1$  is positive for both signs of  $q$ .

In pin-to-plate configurations with interposed dielectric disks as shown in Figure 4,  $\lambda_1(r)$  on the downward-oriented surface of D will generally be bell-shaped, that is, it will have a single maximum at  $r=0$  and approach zero for large  $r$ , see Figure 5 in Section 6 for a confirmation of this expectation for a special geometry.  $\lambda_1(r)$  weights the contributions of annulus-shaped surface charge elements  $2\pi \sigma(r) r \, d r$  to the total induced charge  $Q_1$  which are increasing with decreasing width of  $\sigma_n(r)$ : For given  $q$  and  $\lambda_1(r)$ ,  $Q_1$  is approaching a maximal  $\lambda_1(0) \cdot q$  for a hypothetical delta distribution of charges at  $r=0$ ;  $\lambda_1(0)$  is the upper limit for the ratio  $-Q_1/q$ .

In general,  $\lambda_1$  will be calculated from the distribution of electric potential for an arrangement such as that shown in Figure 4C', by electrostatic field simulation. The corresponding function for electrode 2,  $\lambda_2$ , can then be derived by following consideration: reversing the sign of the potential at electrode 1 ( $\phi_1 = 1 \text{ V} \rightarrow \phi_1 = -1 \text{ V}$ ) reverses the sign of the potential everywhere in the arrangement. If the potential is then increased by 1 V everywhere, the result is  $\lambda_2 = 1 - \lambda_1$  because the potential distribution on the surface D, will also change its sign and be increased

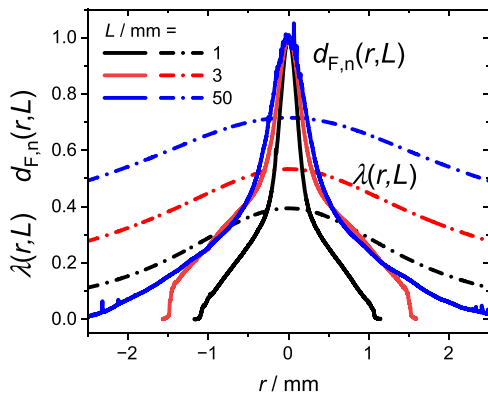


**FIGURE 5** | Graphs of calculated function  $\lambda(r,L)$  on the dielectric's surface. Curves  $d_{F,n}(r,L)$  are measured radial film thickness distributions (see text), normalized by dividing through  $d_F(0,L)$ . Both,  $\lambda(r,L)$  and  $d_{F,n}(r,L)$  show a significant dependence on the length  $L$  of the HV electrode [22].

by 1 V. It follows that  $Q_2 + Q_1 = -q$ : charges on D and on the two electrodes add to zero, as required.

In the following, only electrode 1 is considered and the index 1 of  $Q$ ,  $\lambda$  and  $B$  is dropped. Using  $Q(U)$  plots (Lissajous figures),  $Q(t_{01})$  and  $Q(t_{02})$  can be measured (e.g., see Figure 11I). In general, the normalized charge distribution  $\sigma_n(r)$  and therewith  $B$  are different for surfaces charged positively and negatively by transient discharges with the corresponding polarity,  $\sigma_n^+(r) \neq \sigma_n^-(r)$ . This could already be surmised from the characteristic differences in the famous dust figures produced with “positive electricity” and “negative electricity,” respectively, by G. C. Lichtenberg in Göttingen/Germany in the spring of 1777 [22]. More recently an inequality of  $\sigma_n(r)$  for positive and negative charges was demonstrated in many papers using the electro-optic effect (Pockels effect), for example, see Abolmasov et al. [23] and Stollenwerk et al. [24], and as an application to a pin-to-plate DBD arrangement with a dielectric-covered plate electrode [25]. In asymmetric DBDs, the amounts of positive and negative surface charges at  $U=0$ , too, are not necessarily equal,  $q(t_{01}) \neq -q(t_{02})$  [26]. Therefore assuming that  $q(t_{01}) > 0$  and  $q(t_{02}) < 0$ , the equation for  $\Delta Q_0$  is

$$\Delta Q_0 \equiv Q(t_{02}) - Q(t_{01}) = B^+ q(t_{01}) - B^- q(t_{02}). \tag{15}$$

Equation (15) shows (i) that there is not necessarily a proportionality of  $\Delta Q_0$  and  $\Delta q_0 \equiv q(t_{01}) - q(t_{02})$  and that a difference in the absolute values of  $Q(t_{01})$  and  $Q(t_{02})$  (see Figure 11I as an example) can be due to a difference between  $B^+$  and  $B^-$  and a difference between the absolute values of  $q(t_{01})$  and  $q(t_{02})$  as well, or to both.

It is important to note that  $B^+$  and  $B^-$  are not only dependent on the geometrical design of a setup and the dielectric's permittivity, like electrical capacitances are:  $B^+$  and  $B^-$  generally depend also on the sign of charges and possibly, as in the examples shown below, on experimental parameters such as the fraction  $x_p$  of precursor vapor in a Penning mixture with argon.

## 6 | Preliminary Conclusions From Measured Film Thickness Profiles

If, for axial-symmetric DBD arrangements like in Figure 4, normalized distributions  $\sigma_n^+(r)$  and  $\sigma_n^-(r)$  are known from experiment or simulation, and  $\lambda(r)$  from analytical or numerical calculation,  $B^+$  and  $B^-$  can be calculated from Equation (14) and charges  $q(t_{01})$  and  $q(t_{02})$  can be obtained separately from  $Q(t_{01})$  and  $Q(t_{02})$ . Without any knowledge of charge density distributions, at least the upper limits  $B_{\text{max}}^+ = B_{\text{max}}^- = \lambda(0)$  can be calculated. The latter equations apply exactly for delta distributions of charge at  $r=0$  and are reasonable approximations when the widths of the charge distributions are narrow, compared with the width of the bell-shaped  $\lambda(r)$  as will be shown in the following.

In film deposition experiments motivating the present considerations, the hypothesis may be put forward that (i) film thickness profiles  $d_F(r)$  are due to the time-integrated flux of cations to the dielectric surface D while D is a temporary

cathode [1] and that (ii) the incoming ions first neutralize negative charges, deposited in the previous micro-discharge with a radial dependence  $\sigma^-(r)$ , and (iii) subsequently build up a positive charge density  $\sigma^+(r)$ . Therefore, it appears reasonable to hypothesize that  $d_F(r) \propto \sigma^+(r) - \sigma^-(r)$ , provided that cation fluxes and film formation yield (mass per incoming ions) are the same for ions deposited on negatively and positively charged surfaces<sup>6</sup>. These assumptions do not give the surface charge densities separately but it allows at least to argue that their distributions are not broader than  $d_F(r)$ .

Figure 5 shows  $\lambda(r,L)$  graphs from electrostatic simulations for a pin-to-plate arrangement like it is shown in Figure 11V, with a gap width  $g$  of 2.5 mm, a 1.25-mm thick borosilicate plate (permittivity  $\epsilon = 4.6$ ), and different pin lengths  $L$ . Peak values  $\lambda(0,L)$  are 0.40, 0.53, and 0.72 for  $L = 1, 3,$  and 50 mm, respectively. As mentioned above, these are the maximal ratios  $-Q/q$ , approached for very narrow  $\sigma_n(r)$  distributions.

Radial film thickness profiles  $d_F(r,L)$  were measured on films deposited on the dielectric's surface in an experimental setup with parameters given in Section 1, using 50 ppm HMDS in Ar, flowing through the gap with an average velocity  $v_{av} = 50$  cm/s. The amplitude  $U_0$  of the applied sinusoidal voltage ( $f = 19$  kHz) was chosen 500 V above the  $L$ -dependent extinction voltage; it was  $U_{a,0} = 2.9, 2.2,$  and 1.7 kV for  $L = 1, 3,$  and 50 mm, respectively. In Figure 5, normalized thickness profiles are shown, obtained by dividing through  $d_F(0,L)$ . These profiles are relatively narrow, compared to the bell-shaped  $\lambda(r,L)$ . Over a wide range of radii  $r$ , the thickness profiles can be fitted very well by a sum of two Gaussian functions  $G_1(r,L)$  and  $G_2(r,L)$  with widths ratios  $w_1(L)/w_2(L)$  between about 5 and 6. The narrower component represents only 3% (for  $L = 3$  mm) to 6% (for  $L = 1$  or 50 mm) of the total deposited film volume.

Just to get an impression of  $B^{+/-}$  in this situation, similar distributions were tentatively assumed for  $\sigma^+(r)$  and  $-\sigma^-(r)$ , so that  $\sigma^+(r) \cong -\sigma^-(r) \propto d_F(r)$ . With this assumption,  $B^{+/-} = 0.35, 0.47,$  and 0.64 are obtained for  $L = 1, 3,$  and 50 mm. These results are only 10%–12% smaller than the maximal possible values,  $\lambda(0,L)$  (see above), and to the 2nd digit behind the decimal point independent of the presence of the narrow component  $G_2$ .

The peculiar thickness profiles suggest that there are different deposition mechanisms at work for the narrow and the wide component, respectively. Preliminary infrared-spectroscopic investigations support this conjecture [21]. Further experiments and results of 2D simulations are expected to shed a light on this issue.

## 7 | Summary

The commonly applied analysis of internal DBD parameters (discharge current, gap voltage) in terms of equivalent circuits with three capacitors fails for discharges in setups lacking 2D-translational or cylindrical symmetry. In such cases it is useful to adapt a field-theoretical approach based on the so-called  $\lambda$  function, developed for the analysis of partial discharges in high-voltage systems. Alternatively, a fundamental theorem of

electrostatics can be applied directly, on which the  $\lambda$  function is also based.

In general, the ratio  $B$  of the charges  $Q$ , induced on the electrodes, and the internal charges  $q$ , deposited on the dielectrics by the discharge currents, is not constant like in simple equivalent circuit analyses:  $B$  depends on the distribution of surface charge on dielectrics and thus, for example, on the sign of the charge and on experimental parameters that go beyond the mere geometric design of the setup. In case of the studied pin-to-plate arrangements of electrodes and dielectric, it is sufficient to know the distribution of the electric potential distribution at a certain voltage between the electrodes, to calculate the  $\lambda$  function on the dielectric's surface and from this an upper limit of  $B$ . The actual  $B$  will be close to this limit if the charge density distribution is relatively narrow, compared with the distribution of the  $\lambda$  function on the dielectric's surface, so that charges are mostly deposited close to maximum of the  $\lambda$  function. Beyond that, conclusions or at least conjectures regarding  $B$  are possible if the shapes of charge distributions are known from experiments or simulations, or if reasonable assumptions about the distributions of charges can be made.

## Acknowledgments

The authors are grateful for helpful discussions with Prof. Dr.-Ing. Michael Kurrat, Technische Universität Braunschweig as well as Prof. Dr. Ronny Brandenburg and PD Dr. Detlef Loffhagen, INP, Greifswald. The work is funded by the Deutsche Forschungsgemeinschaft (DFG, German Research Foundation), Project Number: 504701852. Open Access funding enabled and organized by Projekt DEAL.

## Conflicts of Interest

The authors declare no conflicts of interest.

## Data Availability Statement

The data that support the findings of this study are available from the corresponding author upon reasonable request.

## Endnotes

<sup>1</sup>International Electrotechnical Commission

<sup>2</sup>It should be noted that DBDs are always PDs in the electrotechnical sense, as they “only partially bridge the insulation between the conductors,” which consists of gas and dielectric.

<sup>3</sup>Edges of setup I and endings of setup II are neglected. Concentric (spherical) arrangements of conductors are not considered here.

<sup>4</sup>Note that eq. (2) in Pedersen [14] includes space charges but in this brief communication only surface charges on dielectrics are considered. This simplification is possible because in the experiments on which this work is based, discharge currents no longer flow when the applied voltage  $U$  crosses 0, see Figure 11I.

<sup>5</sup>While the name “reciprocity theorem,” used in Griffith' textbook [17], has prevailed in papers published in the recent decade, other monographies use the terms “reciprocal theorem” (see Clemmow [18]) or “reciprocation theorem” (see Smythe [19] or Jackson [20]).

<sup>6</sup>2D simulations are presently under way at INP Greifswald to model charged-particle fluxes and surface charge densities. Expected results may help to decide on the validity of the hypotheses and assumptions used here [27].

## References

1. L. Bröcker, G. S. Perlick, and C.-P. Klages, "Evidence of Ionic Film Deposition From Single-Filament Dielectric Barrier Discharges in Ar-HMDSO Mixtures," *Plasma Processes and Polymers* 17 (2020): 2000129.
2. L. Bröcker, T. Winzer, N. Steppan, J. Benedikt, and C.-P. Klages, "Plasma Polymerization of Allyltrimethylsilane With Single-Filament Dielectric-Barrier Discharges—Evidence of Cationic Surface Processes," *Plasma Processes and Polymers* 21 (2023): 2300177.
3. D. Loffhagen, M. M. Becker, A. K. Czerny, and C. P. Klages, "Modeling of Atmospheric Pressure Dielectric Barrier Discharges in Argon With Small Admixtures of Tetramethylsilane," *Plasma Chemistry and Plasma Processing* 41 (2021): 289–334.
4. R. Brandenburg, "Dielectric Barrier Discharges: Progress on Plasma Sources and on the Understanding of Regimes and Single Filaments," *Plasma Sources Science and Technology* 26 (2017): 053001.
5. W. Hauschild and E. Lemke, *High-Voltage Test and Measuring Techniques* (Berlin, Heidelberg, Germany: Springer-Verlag, 2014).
6. L. Niemeyer, "A Generalized Approach to Partial Discharge Modeling," *IEEE Transactions on Dielectrics and Electrical Insulation* 2 (1995): 510–528.
7. A. P. Jovanović, D. Loffhagen, and M. M. Becker, "Streamer-Surface Interaction in an Atmospheric Pressure Dielectric Barrier Discharge in Argon," *Plasma Sources Science and Technology* 31 (2022): 04LT02.
8. F. J. J. Peeters and M. C. M. van de Sanden, "The Influence of Partial Surface Discharging on the Electrical Characterization of DBDs," *Plasma Sources Science and Technology* 24 (2015): 015016.
9. A. V. Pipa and R. Brandenburg, "The Equivalent Circuit Approach for the Electrical Diagnostics of Dielectric Barrier Discharges: The Classical Theory and Recent Developments," *Atoms* 7 (2019): 14.
10. S. Liu and M. Neiger, "Electrical Modelling of Homogeneous Dielectric Barrier Discharges Under an Arbitrary Excitation Voltage," *Journal of Physics D: Applied Physics* 36 (2003): 3144–3150.
11. R. Brandenburg, M. Schiorlin, M. Schmidt, H. Höft, A. V. Pipa, and V. Brüser, "Plane Parallel Barrier Discharges for Carbon Dioxide Splitting: Influence of Discharge Arrangement on Carbon Monoxide Formation," *Plasma* 6 (2023): 162–180.
12. Z. Cui, Q. Liu, Z. Cai, J. Wang, and Q. Wu, "Modified Equivalent Circuit for Coplanar Dielectric Barrier Discharge Considering Undischarged Areas," *Physics of Plasmas* 30 (2023): 013502.
13. S. Whitehead, *Dielectric Breakdown of Solids* (Clarendon Press, 1951), 171.
14. A. Pedersen, *Annual Report - Conference on Electrical Insulation and Dielectric Phenomena* (IEEE Publication 87CH2462-0, 1987), 58–64.
15. A. Pedersen, G. C. Crichton, and I. W. McAllister, "The Functional Relation Between Partial Discharges and Induced Charge," *IEEE Transactions on Dielectrics and Electrical Insulation* 2 (1995): 535–543.
16. G. C. Crichton, P. W. Karlsson, and A. Pedersen, "Partial Discharges in Ellipsoidal and Spheroidal Voids," *IEEE Transactions on Electrical Insulation* 24 (1989): 335–342.
17. D. J. Griffiths, *Introduction to Electrodynamics* (Prentice-Hall Inc., 1999). 3rd ed, 157–158.
18. P. C. Clemmow, *An Introduction to Electromagnetic Theory* (Cambridge University Press, 1973), 101–107.
19. W. R. Smythe, *Static and Dynamic Electricity* (McGraw-Hill, 1939), 54–55.
20. J. D. Jackson, *Classical Electrodynamics* (John Wiley & Sons Inc., 1999). 3rd ed., 52.
21. L. Bröcker and C.-P. Klages, to be published.
22. J. Takahasi, "Two Hundred Years of Lichtenberg Figures," *Journal of Electrostatics* 6 (1979): 1–13.
23. S. N. Abolmasov, R. Abo, T. Shirafuji, and K. Tachibana, "Spatio-temporal Surface Charge Measurement in Two Types of Dielectric Barrier Discharges Using Pockels Effect," *Japanese Journal of Applied Physics* 45 (2006): 8255–8258.
24. L. Stollenwerk, J. G. Laven, and H.-G. Purwins, "Spatially Resolved Surface-Charge Measurement in a Planar Dielectric-Barrier Discharge System," *Physical Review Letters* 98 (2007): 255001.
25. X. Yang, W. Wang, X. Wang, Y. Du, Y. Meng, and K. Wu, "Experimental Study of Transient Surface Charging During Dielectric Barrier Discharges in Air Gap in Needle-to-Plane Geometry," *Journal of Physics D: Applied Physics* 56 (2023): 465202.
26. L. Stollenwerk and U. Stroth, "Electric Charging in Dielectric Barrier Discharges With Asymmetric Gamma-Coefficients," *Contributions to Plasma Physics* 51 (2011): 61–67.
27. M. Stankov, L. Bröcker, C.-P. Klages, M. M. Becker, and D. Loffhagen, "Hybrid Mode of DBD at Atmospheric Pressure in Ar-HMDS Mixtures: Modelling and Experimental Studies," to be presented at XXXVI ICPIG, July 20–25, 2025.